5

A 1/f Noise Upconversion Reduction Technique

In this chapter, we introduce a method to reduce a flicker (1/f) noise upconversion in voltage-biased RF oscillators. Excited by a harmonically rich tank current, a typical oscillation voltage waveform is observed to have asymmetric rise and fall times due to even-order current harmonics flowing into the capacitive part, as it presents the lowest impedance path. The asymmetric oscillation waveform results in an effective impulse sensitivity function (ISF) of a non-zero dc value, which facilitates the 1/f noise upconversion into the oscillator's $1/f^3$ phase noise. We demonstrate that if the ω_0 tank exhibits an auxiliary resonance at $2\omega_0$, thereby forcing this current harmonic to flow into the equivalent resistance of the $2\omega_0$ resonance, then the oscillation waveform would be symmetric and the flicker noise upconversion would be largely suppressed. The auxiliary resonance is realized at no extra silicon area in both inductor- and transformer-based tanks by exploiting different behavior of inductors and transformers in differential- and common-mode excitations. These tanks are ultimately employed in designing modified class-D and class-F oscillators in 40-nm CMOS technology. They exhibit an average flicker noise corner of less than 100 kHz.

5.1 Introduction

Close-in spectra of RF oscillators are degraded by a flicker (1/f) noise upconversion. The resulting low-frequency phase noise (PN) fluctuations can be mitigated as long as they fall within a loop bandwidth of an enclosing phase-locked loop (PLL). However, the PLL loop bandwidths in cellular transceivers are less than a few tenths to a few hundreds of kHz [1,2], which is below the typical $1/f^3$ PN corner of CMOS oscillators [3–5]. Consequently, a

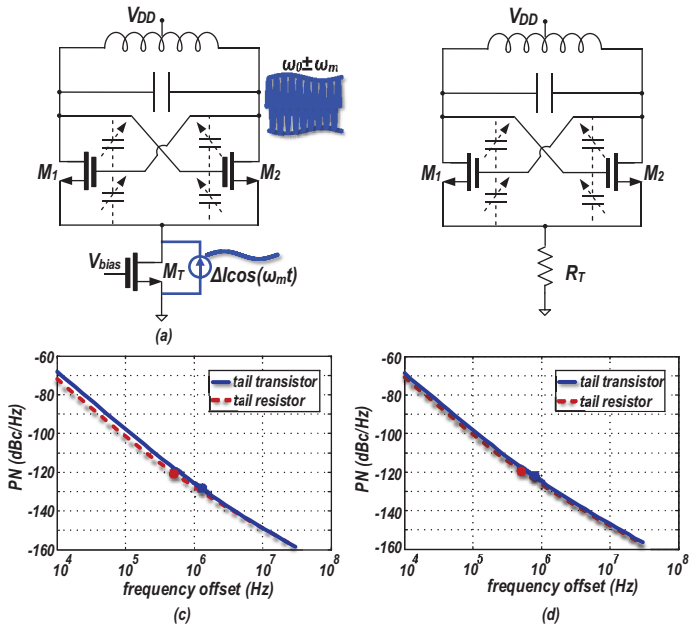

Figure 5.1 Class-B oscillator: (a) with tail transistor $\mathrm{M_T}$; (b) with tail resistor $\mathrm{R_T}$; and their PN when (c) $\mathrm{M_T}$ is always in saturation; (d) $\mathrm{M_T}$ enters partially into triode.

considerable amount of the oscillator's low frequency noise cannot be filtered by the loop and will adversely affect the transceiver operation.

In a current-biased oscillator, flicker noise of a tail transistor, $\mathrm{M_T}$, modulates the oscillation voltage amplitude and then upconverts to PN via an AM–PM conversion mechanism through nonlinear parasitic capacitances of active devices, varactors, and switchable capacitors [6,7] (see Figure 5.1(a)).[1] An intuitive solution is to configure the oscillator into a *voltage-biased* regime, which involves removing the $\mathrm{M_T}$ [8] or replacing it with a tail resistor, $\mathrm{R_T}$, in Figure 5.1(b). Such expected reduction is highly dependent on the tail transistor's operating region. If $\mathrm{M_T}$ in Figure 5.1(a) is always in saturation, the amount of 1/f noise is considerable and the tail resistor $\mathrm{R_T}$ in Figure 5.1(b) could improve the low-frequency PN performance, as shown in Figure 5.1(c). However, in advanced CMOS process nodes with a reduced supply voltage, $\mathrm{M_T}$ partially enters the triode region, thereby degrading the oscillator's effective noise factor but improving the 1/f noise

[1]It is shown in [6] that for certain values of varactor bias voltages, this upconversion is almost eliminated.

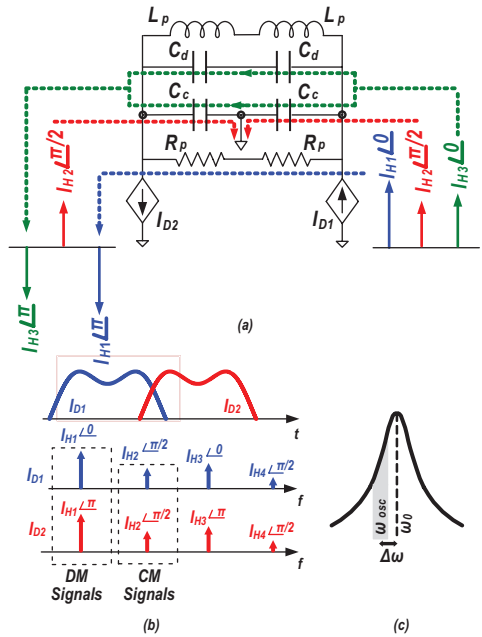

Figure 5.2 (a) Current harmonic paths; (b) drain current in time and frequency domains; (c) frequency drift due to Groszkowski effect.

upconversion; see Figure 5.1(d). In [3], class-C oscillators were designed with a tail transistor and a tail resistor. Measured 1/f^3 corners are almost the same, thus supporting our discussion.[2] However, regardless of the $\mathrm{M_T}$ operating region, removing this source would still not completely eliminate the 1/f noise upconversion.

Another mechanism of the 1/f upconversion is due to Groszkowski effect [10]. In a harmonically rich tank current, the fundamental component, I_{H1}, flows into the equivalent parallel resistance of the tank, R_p. Other components, however, mainly take the capacitive path due to their lower impedance; see Figure 5.2(a). In any balanced RF oscillating circuit, odd harmonics circulate in a differential path, while even harmonics flow in a common-mode path through the resonator capacitance and the switching transistors to ground [32]. Compared to the case with only the fundamental component, the capacitive reactive energy increases by the higher harmonics flowing into them. This phenomenon makes the tank's reactive energy un-balanced.

[2]The actual flicker noise reduction mechanism of class-C oscillators was revealed in [9].

The oscillation frequency will shift down from the tank's natural resonance frequency, ω_0, in order to increase the inductive reactive energy and restore the energy equilibrium of the tank. This frequency shift is given by [11]

$$\frac{\Delta\omega}{\omega_0} = -\frac{1}{Q^2}\sum_{n=2}^{\infty}\frac{n^2}{n^2-1}\cdot\left|\frac{I_{Hn}}{I_{H1}}\right|^2, \tag{5.1}$$

where I_{Hn} is the nth harmonic component of the tank's current. The literature suggests that this shift is static but any fluctuation in I_{Hn}/I_{H1} due to the 1/f noise modulates $\Delta\omega$ and exhibits itself as 1/f^3 PN [12]; see Figure 5.2(c). Although this mechanism has been known for quite some time, it is still not well understood how the flicker noise modifies the I_{Hn}/I_{H1} ratio. Furthermore, (5.1) suggests that all harmonics *indiscriminately* modulate the Groszkowski's frequency shift by roughly the same amount, without regard to their odd/even-mode nature, which could be easily misinterpreted during the study of the flicker noise upconversion in cross-coupled oscillators.

While recognizing the Groszkowski's frequency shift as the dominant physical mechanism in voltage-biased oscillators, we turn our attention to the impulse sensitivity function (ISF) theory in researching the above questions. Hajimiri and Lee [13] have shown that upconversion of any flicker noise source depends on the dc value of the related effective ISF, which can be significantly reduced if the waveform has certain symmetry properties [13, 14]. Another explanation was offered in [15, 16] suggesting that if the 1/f noise current of a switching MOS transistor is to be modeled by a product of stationary noise and a periodic function $w(t)$, then this noise can upconvert to PN if $w(t)$ is asymmetric.

In this chapter, we elaborate on a method proposed in [22, 23, 34] to effectively trap the second current harmonic into a resistive path of a tank in a *voltage-biased* oscillator topology. Doing so will reduce the core transistors' low frequency noise upconversion by making the oscillation waveform symmetric and reducing the effective ISF dc value. We further investigate the effects of harmonics on the core transistors' flicker noise upconversion by studying their impact on the oscillation waveform and on the effective impulse sensitivity function, $\Gamma_{eff,dc}$.

It should be mentioned that several solutions are proposed in literature to reduce the 1/f noise upconversion due to Groszkowski's frequency shift. The concept of a harmonically rich tank current degrading the close-in oscillator spectrum has been noticed for quite some time; however, the proposed solutions mostly include linearization of the system to reduce the level of

current harmonics by limiting the oscillation amplitude by an AGC [17, 18], or linearization of gm-devices [19,20], at the expense of the oscillator's start-up margin and increased 1/f^2 PN. In a completely different strategy, a resistor is added in [21] in series with gm-device drains. An optimum value of the resistor minimizes the flicker noise upconversion; however, the 1/f noise improvement is at the expense of the 20-dB/dec degradation in oscillators with low V_{DD} and high current consumption.

The rest of this chapter is organized as follows. Section 5.2 shows how harmonic components of the drain current contribute to the flicker noise upconversion and shows how an auxiliary CM resonance at $2\omega_0$ mitigates this upconversion. Section 5.3 demonstrates how the auxiliary resonance is realized and proves the effectiveness of the proposed method by implementing two classes of voltage-biased oscillators. Section 5.4 reveals the details of circuit implementations and measurement results.

5.2 Method to Reduce 1/f Noise Upconversion

5.2.1 Auxiliary Resonant Frequencies

Let us start by focusing on reducing the Groszkowski frequency shift. As shown in Figure 5.2(a), the oscillation frequency ω_{osc} fluctuates around the tank's natural resonant frequency ω_0 due to the flow of higher harmonics of the current $I_{D1,2}$ into the capacitive part of the tank. A voltage-biased class-B tank current in time and frequency domains is shown in Figure 5.2(b). Odd harmonics of the tank current are differential-mode (DM) signals; hence, they can flow into both differential- and single-ended capacitors. Even harmonics of the tank current, on the other hand, are common-mode (CM) signals and can only flow into single-ended (SE) capacitors. If the tank possesses further resonances coinciding with these higher harmonics (see Figure 5.3(a)), these components can find their respective resistive path to flow into, as shown in Figure 5.3(b). Consequently, the capacitive reactive energy would not be disturbed and the oscillation frequency shift $\Delta\omega$ would be minimized (see Figure 5.3(c)). The input impedance Z_{in} of such a tank is shown in Figure 5.3(d). The tank has the fundamental natural resonant frequency at ω_0 and auxiliary CM and DM resonant frequencies at even- and odd-order harmonics, respectively. Minimizing the frequency shift $\Delta\omega$ will weaken the underlying mechanism of the 1/f noise upconversion; however, realizing auxiliary resonances at higher harmonics has typically been area inefficient and

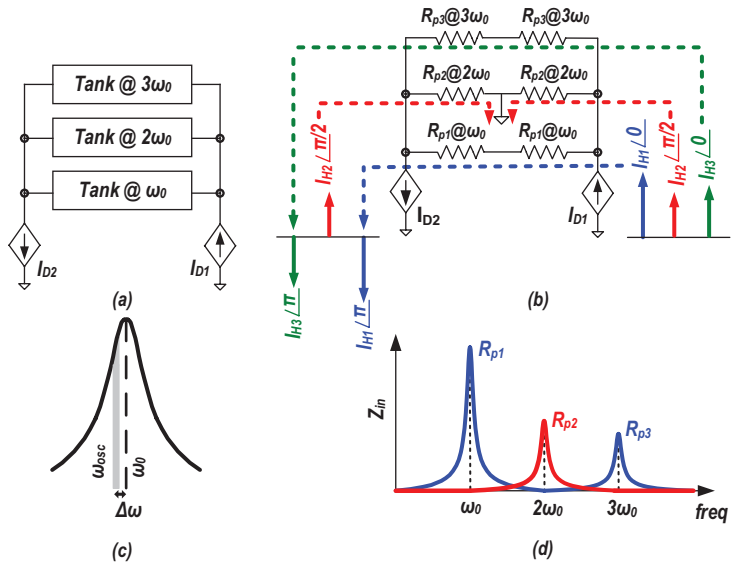

Figure 5.3 (a) Auxiliary resonances at higher harmonics; (b) current harmonic paths; (c) frequency drift; (d) input impedance of the tank.

can also degrade the PN performance. Consequently, the auxiliary resonance frequencies have to be chosen wisely.

Groszkowski frequency shift formula (5.1) indicates that all the contributing current harmonics I_{Hn} are weighted by almost the same coefficients. This means that, in practice, stronger current harmonics I_{Hn} contribute more to the frequency shift. Consequently, we can narrow down the required auxiliary resonances to these harmonics. On the other hand, ultimately, the low frequency noise upconversion depends on the oscillation waveform and the dc value of effective ISF. The various current harmonics contribute unevenly to the flicker noise upconversion since they result in different oscillation waveforms and effective ISF values. Investigating these differences reveals how many and at which frequencies the auxiliary resonances should be realized.

5.2.2 Harmonic Effects on the Effective ISF

A (hypothetical) sinusoidal resonance tank current $I_{H1}(t) = |I_{H1}| \sin(\omega_0 t)$ would result in a sinusoidal resonance oscillation voltage: $V_{H1}(t) = R_{p1} \cdot |I_{H1}| \sin(\omega_0 t) = A_1 \sin(\omega_0 t)$. Its ISF is also a zero-mean sinusoid but

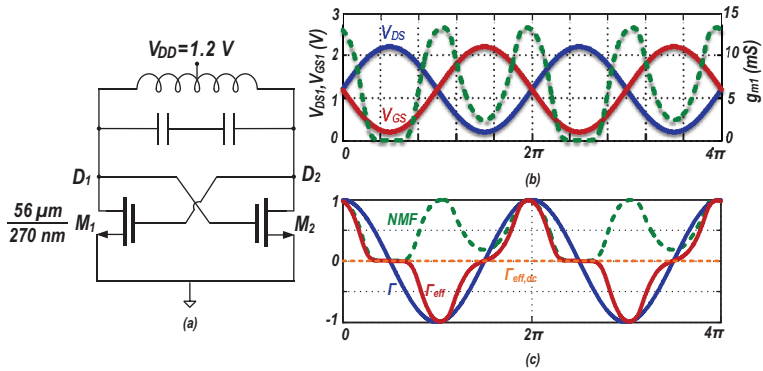

Figure 5.4 Oscillator example: (a) schematic; (b) V_{DS}, V_{GS}, and g_m of M_1 transistor when oscillation voltage contains only fundamental component; (c) its ISF, NMF, and effective ISF.

in quadrature with $V_{H1}(t)$ [24]. The flicker noise of core transistors (e.g., $M_{1,2}$ in Figure 5.4(a)) in a cross-coupled oscillator is modeled by a current source between the source and drain terminals and exhibits a power spectral density as

$$\overline{i_n^2(t)} = \frac{K}{WLC_{ox}} \cdot \frac{1}{f} \cdot g_m^2(\omega_0 t), \tag{5.2}$$

where K is a process-dependent constant, W and L are core transistors' width and length, respectively, and C_{ox} is an oxide capacitance per area. Due to the dependency of current noise on g_m, the flicker noise source is a cyclostationary process and can be expressed as

$$i_n(t) = i_{n0}(\omega_0 t) \cdot \alpha(\omega_0 t), \tag{5.3}$$

in which $i_{n,0}(\omega_0 t)$ shows the stochastic stationarity. $\alpha(\omega_0 t)$ is the noise modulating function (NMF), which is normalized, deterministic, and periodic with maximum of 1. It describes the noise amplitude modulation; consequently, it should be derived from the cyclostationary noise characteristics [13]. In this case, an *effective* impulse sensitivity function is defined as $\Gamma_{eff}(\omega_0 t) = \alpha(\omega_0 t) \cdot \Gamma(\omega_0 t)$. $M_{1,2}$ flicker noise cannot upconvert to PN if effective ISF has a zero dc value.

Let us investigate the $M_{1,2}$ flicker noise upconversion when the oscillation voltage ideally contains only the fundamental component. In Figure 5.4(a), $V_{D1} = V_{DD} - A_1 sin(\omega_0 t)$, $V_{G1} = V_{D2} = V_{DD} + A_1 sin(\omega_0 t)$. Assuming $V_{DD} = 1.2\,\text{V}$ and $A_1 = 1\,\text{V}$, the g_m of the M_1 transistor under such V_{DS} and V_{GS} is found by simulations and is shown as dotted line in Figure 5.4(b).

Under this condition, $\alpha(\omega_0 t) = \frac{g_m(\omega_0 t)}{g_{m,max}}$. ISF, NMF, and the effective ISF of the M_1 flicker noise source are shown in Figure 5.4(c). The dc value of such an effective ISF is zero, resulting in no flicker noise upconversion. This is a well known conclusion and is referred to as a state where $M_{1,2}$ transistors' flicker noise cannot be upconverted to PN [16].

In reality, the tank current of voltage-biased oscillators is rich in harmonics. Due to physical circuit constraints, the even-order current harmonics lead by $\pi/2$, while the odd-order current harmonics are in-phase with the fundamental current I_{H1}. The $\pi/2$ phase difference in even- and odd-order current harmonics considerably changes the oscillation waveform characteristics. For simplicity, we focus only on dominant harmonics, $I_{H2} = |I_{H2}|\sin(2\omega_0 t + \pi/2)$ and $I_{H3} = |I_{H3}|\sin(3\omega_0 t)$, as representatives of even- and odd-order current harmonics, respectively; however, the following discussion can be easily generalized for all harmonics. We also assume for now that the tank only contains SE capacitors.

The differential current I_{H2} flows into the SE capacitors and creates a second-order voltage harmonic:

$$V_{H2}(t) = \frac{1}{C \cdot 2\omega_0} \cdot |I_{H2}| \sin\left(2\omega_0 t + \pi/2 - \pi/2\right) = \alpha_2 A_1 \sin\left(2\omega_0 t\right), \tag{5.4}$$

where the $-\pi/2$ phase shift is due to the capacitive load. The oscillation voltage will then be

$$V_{T2}(t) = V_{H1}(t) + V_{H2}(t) = A_1\left[\sin\left(\omega_0 t\right) + \alpha_2 \sin\left(2\omega_0 t\right)\right]. \tag{5.5}$$

$V_{H1}(t)$, $V_{H2}(t)$, and $V_{T2}(t)$ are plotted in Figure 5.5(a) for $\alpha_2 = 0.1$ and $A_1 = 1\,\text{V}$. $V_{H1}(t)$ has two zero-crossings within its period: at t_1 and t_2, their rise and fall times are symmetric with derivatives: $V'_{H1}(t_1) = -V'_{H1}(t_2)$. V_{H2}'s zero-crossings are also at t_1 and t_2; however, $V'_{H2}(t_1) = V'_{H2}(t_2)$. Consequently, the opposite slope polarities of V_{H1} and V_{H2} at t_1 slow down the fall time of V_{T2}, while the same slope polarities at t_2 sharpen its rise time. Consequently, as can be gathered from Figure 5.5(a), V_{T2} features *asymmetric* rise and fall slopes.

The resulting ISF of the gm transistor is calculated based on (36) in Ref. [13] and is shown in Figure 5.5(b), with its mean dependent on α_2. Larger α_2 leads to more asymmetry between $V_{T2}(t)$ rise and fall slopes; hence, $\Gamma_{eff,dc}$ will increase. Furthermore, repeating the same simulations to obtain g_{m1} with drain and gate voltages that contain second harmonic components results in asymmetric g_{m1} and, consequently, NMF. The slower

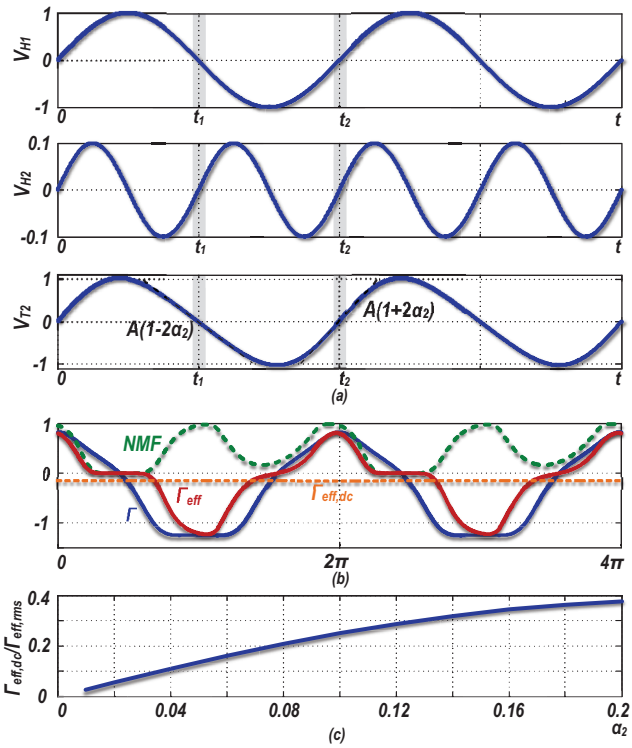

Figure 5.5 Conventional tank waveforms: (a) fundamental, V_{H1}, second harmonic, V_{H2}, voltage components, and oscillation waveform, V_{T2}; (b) its ISF, NMF, and effective ISF; (c) $\Gamma_{eff,dc}/\Gamma_{eff,rms}$ for different α_2 values.

rise/fall times increase the duration when M_1 is turned on, thus widening g_{m1}. A sharper rise/fall time decreases the amount of time when M_1 is turned on, resulting in a narrower g_{m1}. The NMF and effective ISF of such waveforms are shown in Figure 5.5(b). The effective ISF has a dc value which results in $M_{1,2}$'s flicker to PN upconversion. Dependency of the dc value of the effective ISF on α_2 is shown in Figure 5.5(c).

This argument is valid for all even-order current harmonics, and we can conclude that the fluctuations in the even harmonics of the tank's current convert to the $1/f^3$ PN noise through the modulation of the oscillating waveform.

Let us now investigate a case of the tank current containing only odd-harmonic components, with $I_{H3} = |I_{H3}|\sin(3\omega_0 t)$ as a representative. I_{H3}

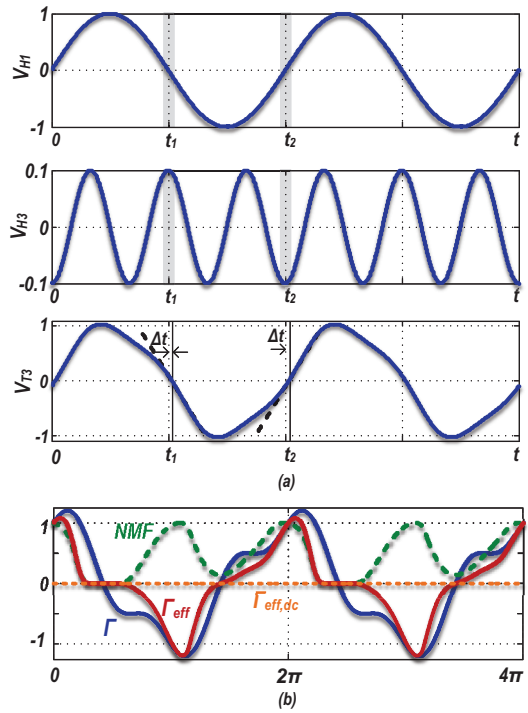

Figure 5.6 Conventional tank waveforms: (a) fundamental, V_{H1}, third harmonic, V_{H3}, voltage component, and oscillation waveform, V_{T3}; (b) its ISF, NMF, and effective ISF.

flows mainly into the tank capacitors and creates a third harmonic voltage as

$$V_{H3}(t) = \frac{1}{C \cdot 3\omega_0} \cdot |I_{H3}| \sin(3\omega_0 t - \pi/2) = \alpha_3 A_1 \sin(3\omega_0 t - \pi/2) \quad (5.6)$$

where, again, the $-\pi/2$ phase shift is due to the capacitive load. The oscillation voltage will then be

$$V_{T3}(t) = V_{H1}(t) + V_{H3}(t) = A_1 \left[\sin(\omega_0 t) + \alpha_3 \sin(3\omega_0 t - \pi/2)\right]. \quad (5.7)$$

$V_{H1}(t)$, $V_{H3}(t)$, and $V_{T3}(t)$ are plotted in Figure 5.6(d) for $\alpha_3 = 0.1$ and $A_1 = 1$ V. It is obvious that the oscillation waveform falling and rising slopes are symmetric, and $\Gamma_{dc} = 0$, as easily gathered from Figure 5.6(e). The simulations show that g_{m1} is slightly asymmetric due to amplitude distortion of the oscillation voltage. However, this asymmetry is canceled out when multiplied by ISF (see Figure 5.6(e)), resulting in an effective ISF with almost zero dc value and thus preventing low-frequency noise upconversion. These

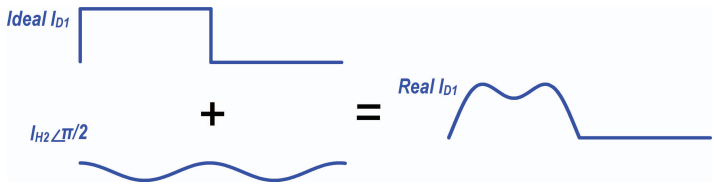

Figure 5.7 Ideal and real current waveforms.

arguments can be generalized for all odd-order harmonics. Consequently, the low-frequency noise of gm transistors does not upconvert to PN if the tank current only contains odd harmonics.

So far, we have assumed $\pi/2$ phase for I_{H2} and π phase for I_{H3}; however, the exact phase shift between the fundamental and harmonic components depends on the transconductor nonlinearity. The ideal drain current in a class-B oscillator is a square wave. However, the core transistors enter triode region, resulting in the real current shape to exhibit a dimple. For this current waveform to appear, a current harmonic with twice the fundamental frequency and $\pi/2$ phase shift has to be added to the original waveform (which only contains odd harmonics), as shown in Figure 5.7. Hence, the phase delay of the second harmonic is not arbitrary but is constrained by the physical circuit. It is worth mentioning that in a class-C oscillator, where the transistors do not enter the triode region, the phase difference between the first and second harmonic is not $\pi/2$. The class-C oscillator shows less $1/f^3$ corner compared to the other topologies which is in agreement with our claim about the importance of the fundamental and second current phase shift on the low frequency noise upconversion. Let us investigate what happens to the voltage waveform and ISF if the fundamental and third-harmonic components are not in-phase, and have a phase shift of ϕ_1. Following the same approach as in the manuscript and assuming $\mathrm{A}_1 = 1, V_{H3} = \alpha_3 \sin(3\omega_0 t - \pi/2 + \phi_1)$. If for $\theta_1 = \omega_0 t_1$, $V_T = V_{H1} + V_{H3} = 0$, then for $\theta_2 = \pi + \theta_1$, $V_T = \sin(\theta_2) + \alpha_3 \sin(3\theta_2 + \phi_1) = -\sin(\theta_1) - \alpha_3 \sin(3\theta_1 + \phi_1) = 0$. Then the V_T slopes at θ_1 and θ_2 would be

$$\begin{aligned} V_T'(\theta_1) &= \cos(\theta_1) + 3\alpha_3 \cos(3\theta_1 + \phi_1) \\ V_T'(\theta_2) &= \cos(\pi + \theta_1) + 3\alpha_3 \cos(3\pi + 3\theta_1 + \phi_1) = -V_T'(\theta_1). \end{aligned} \quad (5.8)$$

Consequently, regardless of the exact phase difference between the current's fundamental and third-harmonic components, the oscillation voltage in the presence of third (and, in general, odd) harmonics would have symmetric

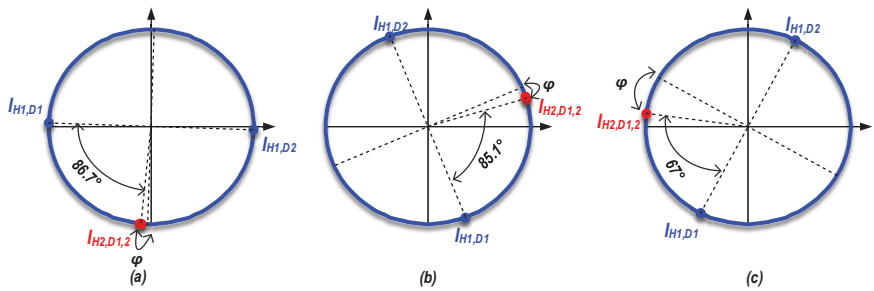

Figure 5.8 Tank's current fundamental and second-harmonic phases in (a) class-D; (b) class-F_3; and (c) class-C topologies.

rise and fall times, and consequently they will not be responsible for 1/f to phase noise upconversion.

For the second-harmonic component, the story is entirely different. The most asymmetric rise and fall times of the oscillation voltage waveform happen when the fundamental and second-harmonic current components have exactly the $\pi/2$ phase difference. However, if the phase difference is not exactly $\pi/2$ (and it is, for example, $\pi/2 - \phi_1$), rise and fall times are still asymmetric and the ISF still contains a non-zero dc value. The proposed method would be still effective not at exactly $\omega_{CM} = 2\omega_0$, but at a CM resonance that has the $\phi_1 - \pi/2$ phase at $2\omega_0$ and cancels out the extra phase difference, ϕ_1, therefore, resulting in a completely symmetric rise and fall times. It is worth mentioning that if ϕ_1 were originally close to $\pi/2$, the oscillation waveform should have theoretically very symmetric rise and fall times. However, due to the real-world circuit constraints, that situation could not be reproduced in simulations.

Independent from the above explanations, we did some circuit-level simulations to show exact phase shift of the second harmonic compared to the fundamental components in class-D, class-F_3, and also class-C topologies. The results are shown in Figure 5.8. For class-D and class-F_3 topologies, the $\pi/2$ phase difference appears to be a very good estimation. However, as predicted for the class-C topology, $\pi/2$ phase difference is not a precise estimation.

To further support that 1/f noise upconverts more to PN if α_2 is increased, we tried to run some simulations on the voltage-biased class-B oscillator of Figure 5.9(a). Controlling the second-harmonic current is not very straightforward. It can be modified by changing the core transistors' width, W, or by changing tank's quality factor, Q. In both of these methods, the oscillation

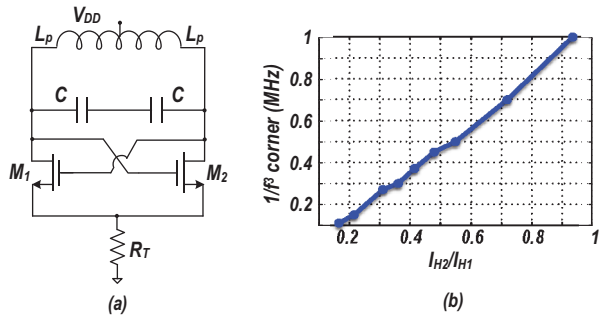

Figure 5.9 (a) Voltage-biased class-B oscillator schematics; (b) $1/f^3$ corner versus I_{H2}/I_{Hn}.

waveform amplitude would get affected. If we fix the oscillation amplitude when W or Q are swept, the second harmonic power modification range becomes very limited. On the other hand, by changing the transistors' width, the flicker noise of the device also changes and adds another parameter. Consequently, in the following simulations, we swept the tank quality factor, and all the other parameters, such as transistor sizes, supply voltage, etc., are kept the same. With higher Q, the oscillation voltage increases, the device spends more time in triode region and becomes more non-linear, consequently generating more current harmonics. M_1 and M_2 in the class-B oscillator are thick-oxide 56µ/270n devices, $V_{DD} = 1.2V$, $R_T = 9$ Ohm. The capacitors are ideal and not tunable. The simulation results are shown in Figure 5.9(b). As we have discussed the flicker noise upconversion depends on the α_2 value, which is proportional to the I_{H2}/I_{Hn} ratio. Therefore, we reported the $1/f^3$ corner versus I_{H2}/I_{Hn}, and it is obvious from Figure 5.9(b) that the corner increases for larger I_{H2}/I_{Hn} ratios in this class-B oscillator.

5.2.3 Resonant Frequency at $2\omega_0$

Thus far, we have shown that the even components of the tank's current are chiefly accountable for the asymmetric oscillation waveform and the 1/f noise upconversion to PN. Let us investigate what happens to the oscillation waveform and effective ISF if the tank has an auxiliary CM resonance at $2\omega_0$. Such resonance provides a resistive (i.e., via R_{p2}) path for I_{H2} to flow into it, and hence the voltage second-harmonic component is

$$V_{H2,aux}(t) = R_{p2}|I_{H2}|\sin(2\omega_0 t + \pi/2) = A_1\alpha_{2,aux}\sin(2\omega_0 t + \pi/2)\,. \tag{5.9}$$

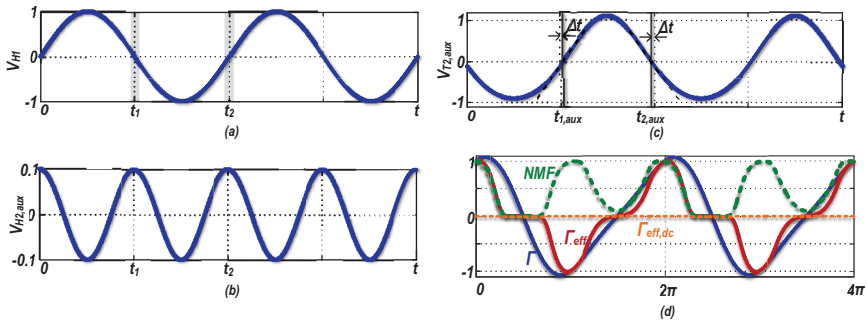

Figure 5.10 Proposed tank waveforms: (a) fundamental voltage component, V_{H1}; (b) voltage second harmonic in the presence of auxiliary resonance, $V_{H2,aux}$; (c) oscillation waveform, $V_{T2,aux}$; (d) its ISF, NMF, and effective ISF.

The composite oscillation voltage will become

$$\begin{aligned} V_{T2,aux}(t) &= V_{H1}(t) + V_{H2,aux}(t) \\ &= A_1 \left[\sin(\omega_0 t) + \alpha_{2,aux} \sin(2\omega_0 t + \pi/2)\right]. \end{aligned} \tag{5.10}$$

$V_{H1}(t)$, $V_{H2,aux}(t)$, and $V_{T2,aux}(t)$ are plotted in Figure 5.10(a,b,c) for $\alpha_{2,aux} = 0.1$ and $A_1 = 1$. The rise and fall times of the oscillation voltage are now symmetric (see Figure 5.10(c)) and so the ISF is zero mean, as shown in Figure 5.10(d). g_{m1}, and thus NMF, are also completely symmetrical; consequently, the effective ISF has a zero dc value, preventing low-frequency noise from being upconverted. The oscillation waveform is still dependent on $\alpha_{2,aux}$, but the rise and fall times are always symmetric, thus keeping $\Gamma_{eff,dc}$ zero.

The second and third current harmonics are the most dominant in all classes of oscillators, so α_2 and α_3 are significantly larger than other α_n for $n = 4, 5, \ldots$. Meanwhile, Γ_{dc} is a growing function of α_n for $n = 2k$, where $k = 1, 2, \ldots$. We can, therefore, conclude that I_{H2} is the main contributor to the 1/f noise upconversion. Consequently, attention to only one auxiliary resonant frequency at $2\omega_0$ appears sufficient [22, 26, 27].

5.2.4 ω_{CM} Deviation from $2\omega_0$

The balance in the rise and fall zero-crossing slopes in Figure 5.10(c) is rooted in the $\pi/2$ phase shift between $V_{H1}(t)$ and $V_{H2}(t)$. This is a combination of the $\pi/2$ phase difference between $I_{H1}(t)$ and $I_{H2}(t)$ and zero phase of the

resistive tank impedance at $2\omega_0$. When ω_{CM} deviates from $2\omega_0$

$$\begin{aligned} V_{T2,aux}(t) &= V_{H1}(t) + V_{H2,aux}(t) \\ &= R_{p1}|I_{H1}|\sin(\omega_0 t) + |Z_{CM}| \cdot |I_{H2}| sin(2\omega_0 t + \pi/2 + \phi_{CM}) \\ &= A_1 [\sin(\omega_0 t) + \alpha_{2,aux} sin(2\omega_0 t + \pi/2 + \phi_{CM})] \end{aligned} \tag{5.11}$$

where $|Z_{CM}|$ and ϕ_{CM} are the CM input impedance magnitude and phase, respectively, derived as,

$$\phi_{CM} = \arctan\left(\frac{1-\zeta^2}{\frac{\zeta}{Q_{CM}}}\right) \tag{5.12}$$

$$|Z_{CM}| = R_{p2} \cdot \frac{\frac{\zeta}{Q_{CM}}}{\sqrt{(1-\zeta^2)^2 + \left(\frac{\zeta}{Q_{CM}}\right)^2}} \tag{5.13}$$

where $\zeta = \frac{2\omega_0}{\omega_{CM}}$. The ω_{CM} versus $2\omega_0$ misalignment has two effects. The first directly translates ϕ_{CM} into the waveform asymmetry. Figure 5.11(a) shows $V_{T2,aux}(t)$ for different ϕ_{CM}; $\alpha_{2,aux}$ was chosen as 0.3 to better illustrate the asymmetry. When grossly mistuned from $2\omega_0$, ϕ_{CM} could approach $\pm\pi/2$, thus making the auxiliary resonance completely ineffective. A larger Q-factor of the common-mode resonance, Q_{CM}, results in ϕ_{CM} closer to $\pm\pi/2$ for the same $2\omega_0/\omega_{CM}$ ratios, as illustrated in Figure 5.11(b).

The second effect is due to $\alpha_{2,aux}$, which determines the amount of second harmonic in the voltage waveform. When ϕ_{CM} is not zero, $\Gamma_{eff,dc}$ becomes dependent on $\alpha_{2,aux}$: the larger $\alpha_{2,aux}$, the more asymmetric waveform and more 1/f noise upconversion. The $\alpha_{2,aux}$ value can be found from the following equation:

$$\alpha_{2,aux} = \left|\frac{I_{H2}}{I_{H1}}\right| \cdot \frac{|Z_{CM}|}{R_{p1}}. \tag{5.14}$$

I_{H2}/I_{H1} is dependent on the oscillator's topology. Furthermore, the larger Q_{CM}, the larger R_{p2} and hence the larger $\alpha_{2,aux}$. Figure 5.11(c) shows the expected $\Gamma_{eff,dc}/\Gamma_{eff,rms}$ versus ϕ_{CM} for different $\alpha_{2,aux}$. Both of these effects point out that Q_{CM} should be low to reduce the sensitivity of this method to the ω_{CM} deviation from $2\omega_0$. Parsitic inductances and capacitances between supply and groud rails can contribute to this deviation. This parasitics become especially important at mmW frequencies [25].

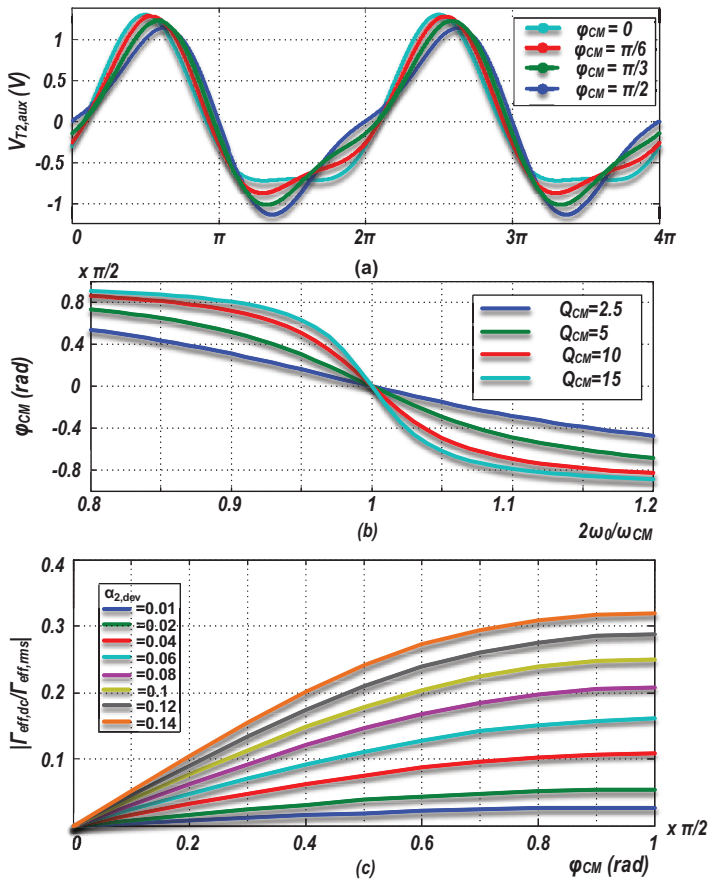

Figure 5.11 (a) $V_{T2,aux}$ for different ϕ_{CM}; (b) ϕ_{CM} for different Q_{CM} when ω_{CM} deviates from $2\omega_0$; (c) $\Gamma_{eff,dc}/\Gamma_{eff,rms}$ for different $\alpha_{2,aux}$ and ϕ_{CM}.

5.3 Circuit Implementation

We have shown that if the tank demonstrates an auxiliary CM resonance at the second harmonic of its fundamental ω_0 resonance, the oscillation waveform would be symmetric and, hence, the flicker noise upconversion would be suppressed. Since the differential capacitors are not seen by the CM signals (i.e., I_{H2}), a straightforward solution for realizing a CM peak is to design a tank as demonstrated in Figure 5.12(a)) with a set of differential C_d and single-ended (SE) C_c capacitors [26,27]. r_p is the equivalent series resistance of the inductor and it is assumed that all capacitors are nearly ideal. This tank

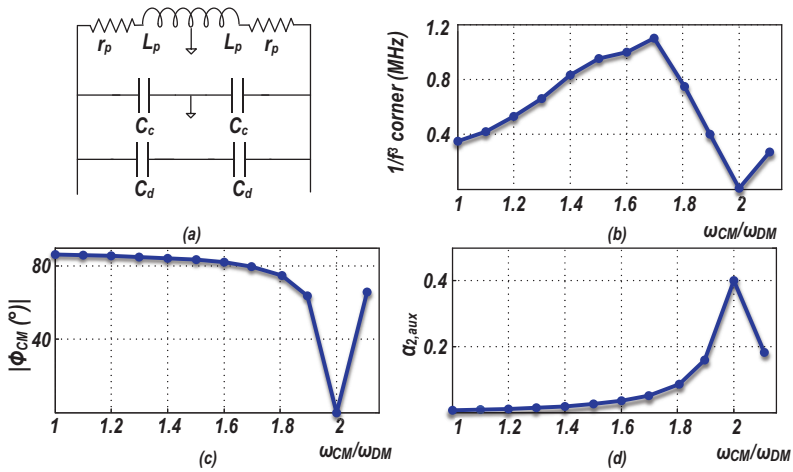

Figure 5.12 (a) A tank with DM and CM resonances; (b) 1/f^3 corner of the oscillator employing this tank; (c) ϕ_{CM}; and (d) $\alpha_{2,aux}$ of the tank versus ω_{CM}/ω_{DM}.

shows a fundamental DM resonant frequency, $\omega_{DM} = \frac{1}{\sqrt{L_p(C_c+C_d)}}$ and a CM resonant frequency $\omega_{CM} = \frac{1}{\sqrt{L_pC_c}}$. From (5.12)–(5.14):

$$\phi_{CM} = \arctan\left(\frac{1-\frac{4C_c}{C_c+C_d}}{\frac{1}{Q_{DM}}\cdot\frac{2C_c}{C_c+C_d}}\right) \tag{5.15}$$

$$\alpha_{2,aux} = \frac{R_{p2}}{R_{p1}}\cdot\frac{\frac{2}{Q_{DM}}\cdot\left(\frac{C_c}{C_c+C_d}\right)}{\sqrt{\left(1-\frac{4C_c}{C_c+C_d}\right)^2+\left(\frac{2}{Q_{DM}}\cdot\frac{C_c}{C_c+C_d}\right)^2}}\cdot\frac{I_{H2}}{I_{H1}}, \tag{5.16}$$

where Q_{DM}, R_{p2}, and R_{p1} are, respectively, the quality factor at DM resonance, and impedance peaks at CM and DM resonances. In an extreme condition of $C_d = 0$, the tank contains only the SE capacitors and reduces to a conventional tank discussed in Section 5.2.2. Targeting $\omega_{CM} = 2\omega_{DM}$ results in $C_d = 3C_c$ and we can prove that $Q_{CM} = 2Q_{DM}$. As discussed supra, the fairly large Q_{CM} exacerbates the effects of CM resonance misalignment.

To investigate the effectiveness of the proposed method on the tank mistuning sensitivity, we performed an analysis of a 5-GHz voltage-biased class-B oscillator of Figure 5.1(b) with $Q_{DM} = 10$. The oscillator is designed in a 40-nm CMOS technology, and $M_{1,2}$ are thick-oxide (56/0.27)-μm devices. The power consumption is 10.8 mW at $V_{DD} = 1.2$ V. As

expected, the 1/f^3 corner of this oscillator is at its minimum of ∼10 kHz at $C_d/C_c = 3$ (see Figure 5.12(b)). When ω_{CM} deviates from $2\omega_{DM}$, i.e., C_d/C_c ratio deviates from the ideal value of 3, while keeping $C_c + C_d$ constant, the 1/f^3 corner starts to increase from the 10 kHz minimum and reaches its peak at $\omega_{CM} = 1.7\omega_{DM}$ when the CM resonance phase, ϕ_{CM}, gets close to $\pi/2$ (about 80° as shown in Figure 5.12(c)). After this point, the ϕ_{CM} barely changes, but $\alpha_{2,aux}$ decreases (Figure 5.12(d)) and, consequently, the 1/f^3 corner reduces again. The maximum 1/f^3 corner of 1.1 MHz is actually much worse than the 400 kHz corner of extreme case when $C_d = 0$ (see Figure 5.12(b)). This means that if the tank is not designed properly, the performance would be even worse than that without applying this technique. Consequently, to ensure no performance degradation in face of the misalignment, $\alpha_{2,aux}$ at $\phi_{CM} \approx 80°$ should be less than that of the tank without the applied technique. α_2 when $C_d = 0$ can be found from (5.16):

$$\alpha_2 \approx \frac{2}{3Q_{DM}} \cdot \frac{I_{H2}}{I_{H1}} \tag{5.17}$$

$\phi_{CM} = 80°$, (5.15) and (5.16) result in

$$\alpha_{2,aux} = \frac{R_{p2}}{R_{p1}} \cdot \frac{\tan\left(\frac{\pi}{18}\right)}{\sqrt{1+\tan^2\left(\frac{\pi}{18}\right)}} \cdot \frac{I_{H2}}{I_{H1}}. \tag{5.18}$$

Hence,

$$\frac{R_{p2}}{R_{p1}} < \frac{3.84}{Q_{DM}} \tag{5.19}$$

to satisfy this condition, which results in non-practical Q_{DM} values.

In the following two subsections, we show how to substantially reduce the sensitivity to such misalignment by employing, at no extra area penalty, an inductor exhibiting distinct and beneficial characteristics in DM and CM excitations. The different behavior of a 1:2 turn transformer in DM and CM excitations is also exploited to design a transformer-based F_2 tank. With these new tanks, we construct class-D and a class-F oscillators to demonstrate the effectiveness of the proposed method of reducing the flicker noise upconversion. Before we do that, let us compare the 1/f^3 corner and current harmonics of a current-biased class-B (see Figure 5.13(a)), a current-biased class-B with noise filtering technique [32] applied to it (see Figure 5.13(b)), and a voltage-biased class-B with the proposed technique applied to it (see Figure 5.13(c)). In the current-biased configuration proposed in [32], a capacitor in parallel with the current source shorts noise frequencies around $2\omega_0$

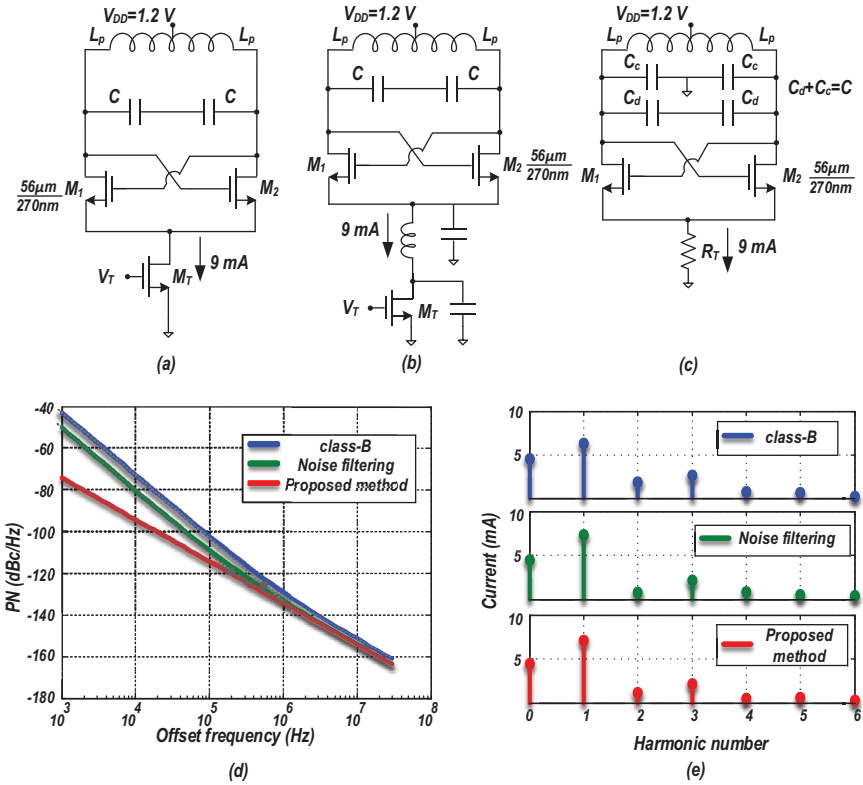

Figure 5.13 (d) PN and (e) current harmonic components of a class-B oscillator (a), and similar counterparts with noise filtering technique [32] (b) and the proposed method applied (c).

to ground. An inductor is interposed between the common source of the cross-coupled transistors and the current source. That inductor resonates at $2\omega_0$ with the equivalent capacitor at the common source of the oscillator transistors (see Figure 5.13(b)). The purpose of that resonator is creating a high impedance path at $2\omega_0$ to stop the tank loading when one of the core transistors enters the triode region. That method is also partially effective in reducing low-frequency noise upconversion of core transistors by linearizing the core transistors and reducing current harmonics, especially the second-harmonic component content. That resonator has to be tunable over the tuning range and it increases the die area. Figures 5.13(d–e) show the PN performance and current harmonic components of the three oscillators shown in Figure 5.13(a–c). In the simulations, all the capacitors are ideal capacitors

and non-tunable. It is obvious how much the second-harmonic current is reduced in the noise filtering method, and consequently the $1/f^3$ corner is lower than that in a conventional class-B oscillator.

5.3.1 Inductor-Based F_2 Tank

Figures 5.14(a,b) show a 2-turn "F_2" inductor when it is excited by DM and CM signals. In the DM excitation, currents in both turns have the same direction, resulting in an additive magnetic flux. However, in the CM excitation, currents have opposite direction and cancel each other's flux [28]. With the proper spacing between the F_2 inductor windings, effective inductance in CM can be made 4x smaller than that in DM. The L_{DM}/L_{CM} inductance ratio is controlled through lithography that *precisely* sets the physical inductor dimensions and, consequently, makes it *insensitive* to process variations.

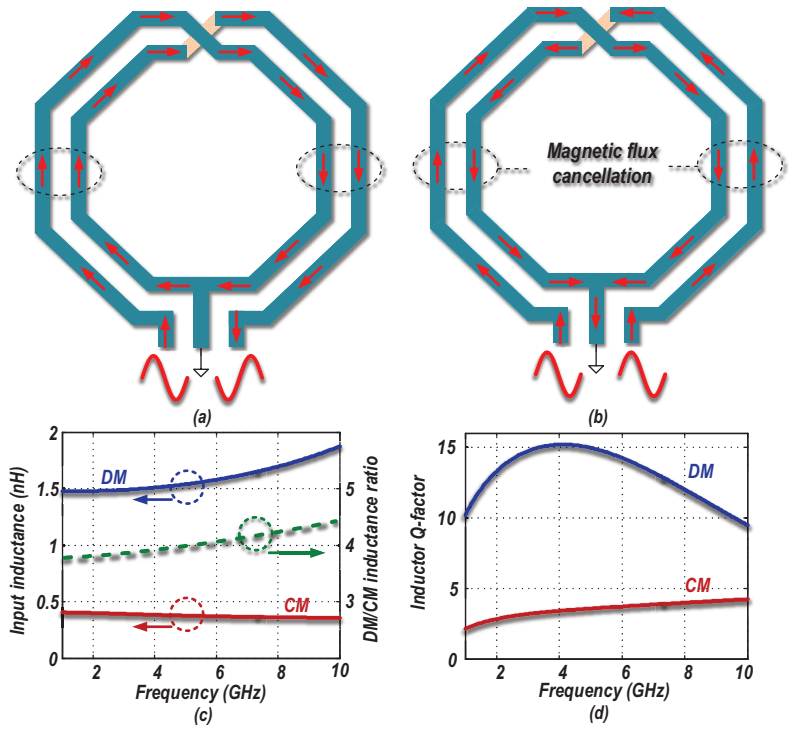

Figure 5.14 A 2-turn "F_2" inductor in (a) DM excitation; (b) CM excitation; (c) F_2 DM and CM inductances and their ratio; (d) Q_{DM} and Q_{CM}.

Figure 5.14(c) shows the DM and CM inductances and their ratio over frequency. L_{DM}/L_{CM} is close to 4 within a 30%–40% tuning range.

Differential capacitors cannot be seen by the CM signals; hence, to be able to set the CM resonance, the F_2 tank capacitors should be SE, as shown in Figure 5.15(a). The F_2 tank demonstrates two resonant frequencies: ω_{DM} and ω_{CM}. Both of these are tuned simultaneously by adjusting C_c. The precise inductor geometry maintains $L_{DM}/L_{CM} \approx 4$ and hence $\omega_{CM}/\omega_{DM} \approx 2$ over the full tuning range.

The input impedance of the tank is shown in Figure 5.15(b). Presuming the capacitance losses are negligible, the DM and CM resonance quality factors are

$$Q_{DM} = \frac{L_p \omega_{DM}}{r_p} = Q_0 \tag{5.20}$$

$$Q_{CM} = \frac{L_p \omega_{CM}}{4 r_p} = \frac{Q_0}{2}. \tag{5.21}$$

The Q-factor of the CM resonance is half that of DM, which relaxes the F_2 tank sensitivity to mismatch between ω_{CM} and $2\omega_{DM}$. For this inductor-based F_2 tank, $R_{p2}/R_{p1} = 0.25$ and the condition in (5.19) is *satisfied* for $Q_0 < 15$. Furthermore, in the CM excitation, the currents in adjacent windings have opposite direction, which results in an increased AC resistance [29] and so the Q-factor of the CM inductance is even smaller than in (5.21). The Q-factor of L_{CM} inductance of Figure 5.14(b) is about 3–4.

Apart from the easy tuning with only one capacitor bank, the mostly SE parasitic capacitors do not play any role in defining the $\omega_{CM}/2\omega_{DM}$ ratio.

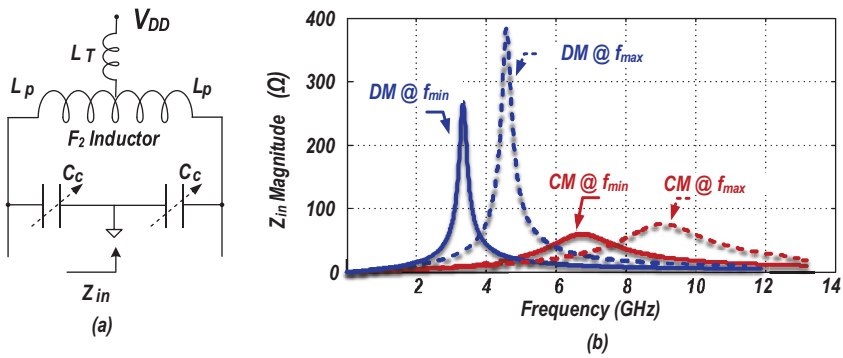

Figure 5.15 (a) Inductor-based F_2 tank and (b) its input impedance.

Furthermore, the low Q_{CM} and, consequently, the lower sensitivity to the $\omega_{CM}/2\omega_{DM}$ ratio that the inductor-based F_2 tank offers make it all more attractive than the tank shown in Figure 5.12(a).

5.3.2 Class-D/F_2 Oscillator

Among the various classes of inductor-based oscillators (e.g., class-B, complementary class-B, class-D [4]), we have decided to validate the proposed method on a class-D oscillator depicted in Figure 5.16(a). This recently introduced oscillator shows promising PN performance in the $1/f^2$ region due to its special ISF. The tail current transistor is removed there and wide and almost ideal switches $M_{1,2}$ clip the oscillation voltage to GND for half a period (see Figure 5.16(b)) resulting in an almost zero ISF there

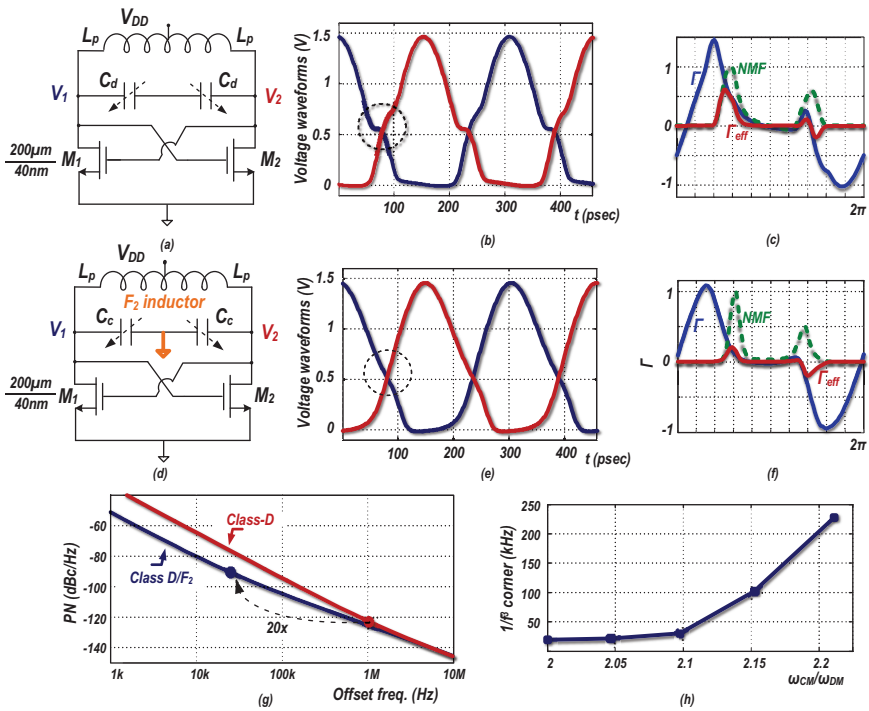

Figure 5.16 Class-D oscillator: (a) schematic; its (b) waveforms; and (c) gm-transistor ISF, NMF, and effective ISF. Class-D/F_2 oscillator: (d) schematic; its (e) waveforms; and (f) gm-transistor ISF, NMF, and effective ISF; (g) their PN performance; and (h) 1/f^3 corner sensitivity to ω_{CM}/ω_{DM}.

(Figure 5.16(c)). However, the hard clipping of the drain nodes to GND generates a huge amount of higher-order harmonic currents. Due to the large I_{H2}, in agreement with our analysis, the oscillating waveform has asymmetric fall and rise times (clearly visible in Figure 5.16(b)) and it exhibits a strong 1/f noise upconversion and frequency pushing. A version of class-D with a tail filter technique [32] was also designed in [4] in an attempt to reduce the low frequency noise upconversion. This method is partially effective, lowering the $1/f^3$ PN corner from 2 to 0.6–1 MHz. Due to the above reasons, this voltage-biased oscillator seems a perfect fit for the proposed method.

Figure 5.16(d) shows the proposed class-D/F_2 oscillator, which adopts the F_2 tank. The gm-devices, M_1 and M_2, still inject a large I_{H2} current into the tank, but this current is now flowing into the equivalent resistance of the tank at $2\omega_0$. Clearly, the rise/fall times are more symmetric in the class-D/F_2 oscillator, as demonstrated in Figure 5.16(e). The gm-transistors' ISF, NMF, and effective ISF are shown in Figure 5.16(f). As predicted, effective Γ_{dc} is now reduced and the simulated PN performance shows that the $1/f^3$ corner is lowered from 1 MHz to ∼30 kHz (Figure 5.16(g)).

The parasitic inductance L_T has to be considered in designing the F_2 inductor. C_c controls both CM and DM resonant frequencies simultaneously; hence, any deviation of ω_{CM} from $2\omega_0$ is due to L_{CM}/L_{DM} not being exactly 4 over the TR. To examine the robustness of the tank via simulations, a C_d differential capacitor is deliberately added to the tank. $C_c + C_d$ is kept constant in order to maintain the oscillation frequency. This capacitor shifts down ω_{DM} while keeping ω_{CM} intact. Figure 5.16(h) shows how the $1/f^3$ corner worsens when C_d/C_c ratio increases. The class-D/F_2 oscillator is quite robust to process variations. First of all, due to the low CM resonance quality factor of an F_2 inductor, this topology is less sensitive to deviations of ω_{CM} from $2\omega_0$. Furthermore, in this topology, only single-ended capacitor banks are employed; hence, ω_{CM}/ω_{DM} ratio is solely defined by L_{CM}/L_{DM}. The cross-coupled transistor's parasitic capacitors are mostly single-ended, except for C_{gd} which is less than 5% of the tank's total capacitance. Consequently, the modification of core transistors' parasitic capacitance over process variations will only change oscillation frequency and barely modify the ω_{CM}/ω_{DM} ratio. Figure 5.17(a) shows simulation results for the $1/f^3$ corner of the class-D/F_2 oscillator in different process corners. The PN at 10-kHz offset frequency for both class-D/F_2 oscillators for 200 points Monte Carlo simulations on inter/intra die process variations is shown in Figure 5.17(a).

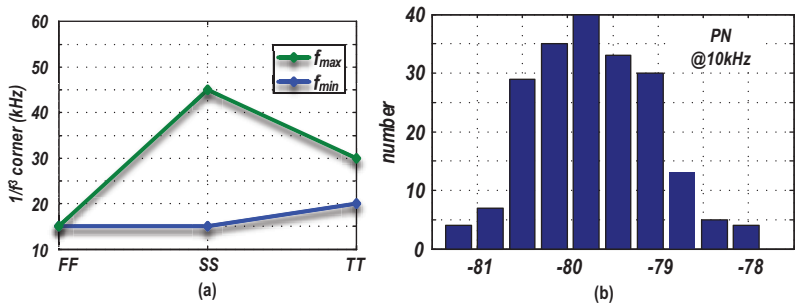

Figure 5.17 Class-D/F_2 oscillator: $1/f^3$ corner over process variation and (b) histogram of PN at 10-kHz offset frequency.

5.3.3 Transformer-Based F_2 Tank

Figures 5.18(a,b) show a 1:2 turns transformer excited by DM and CM input signals at its primary. With a DM excitation, the induced currents at the secondary circulate in the same direction leading to a strong coupling factor, k_m. On the other hand, in CM excitation, the induced currents cancel each other, resulting in a weak k_m [30]. The latter means that the secondary winding cannot be seen by the CM signals. "F_2" transformer-based tank is shown in Figure 5.19(a).

At the DM excitation, no current flows into the metal track inductance, L_T, that connects the center tap to the supply's AC-ground

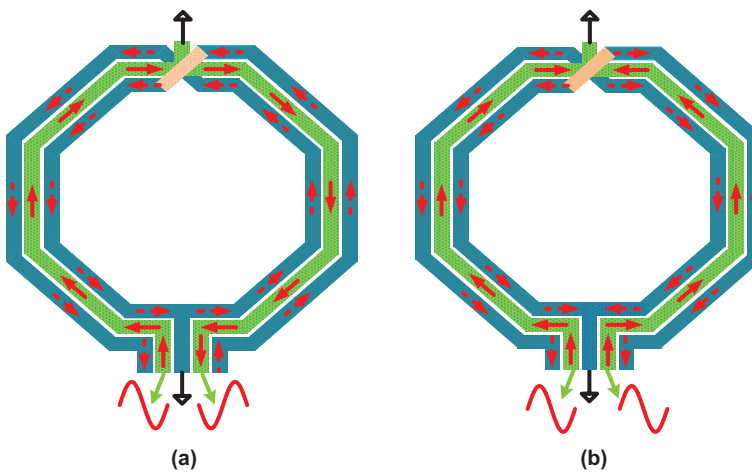

Figure 5.18 1:2 transformer when the primary is excited with (a) DM and (b) CM currents.

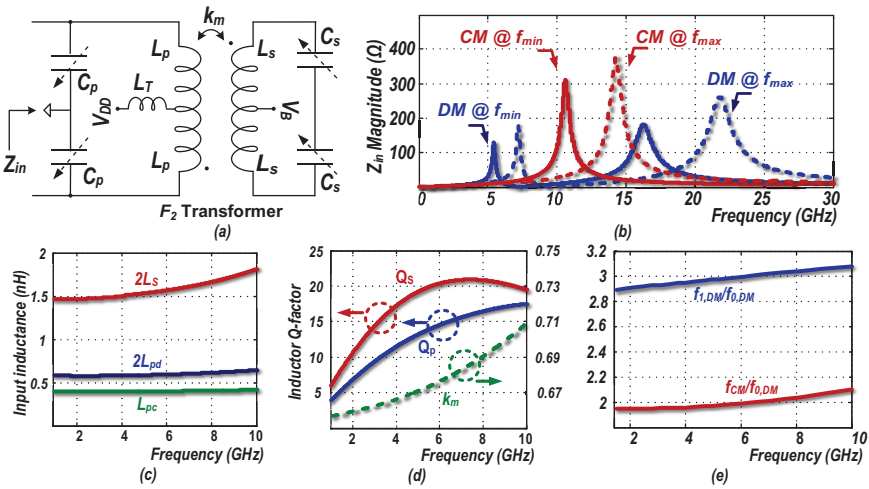

Figure 5.19 (a) Transformer-based F_2 tank; (b) its input impedance; (c) DM and CM primary and secondary inductance; (d) primary and secondary inductance quality factor and coupling factor; (e) DM and CM resonant frequencies over TR.

(see Figure 5.19(a)). However, at the CM excitation, the current flowing into L_T is twice the current circulating in the inductors. Consequently, the tank inductance L_p in Fig. 5.19(a) is re-labeled as $L_{pd} = L_p$ in DM and $L_{pc} = L_{pd} + 2L_T$ in CM excitations. This tank employs SE primary and differential secondary capacitors and demonstrates two DM and one CM resonant frequencies. $\omega_{CM} = 1/\sqrt{L_{pc}C_p}$ and if $k_{m,DM}$>0.5, $\omega_{0,DM} = 1/\sqrt{L_{pd}C_p + L_sC_s}$ [5]. F_2 tank requires $\omega_{CM} = 2\omega_{0,DM}$; hence,

$$L_sC_s = C_p(4L_{p,c} - L_{p,d}). \tag{5.22}$$

Unlike in the inductor-based tank, here, the $\omega_{CM}/\omega_{0,DM}$ ratio is dependent on the secondary-to-primary capacitor ratio. Furthermore, the input impedance Z_{in}, shown in Figure 5.19(b), reveals that Q_{CM} is not low, thus making it sensitive to $\omega_{CM}/\omega_{0,DM}$. It means the C_s/C_p ratio has to be carefully designed to maintain $\omega_{CM}/\omega_{0,DM} \approx 2$ over the tuning range. In practice, the Q-factor of capacitor banks is finite and decreases at higher frequencies, so Q_{CM} will reduce, thus making the tank a bit less sensitive.

5.3.4 Class-$F_{2,3}$ Oscillator

As proven in [5], a DM auxiliary resonance at the third harmonic of the fundamental frequency is beneficial in improving the 20-dB/dec PN performance

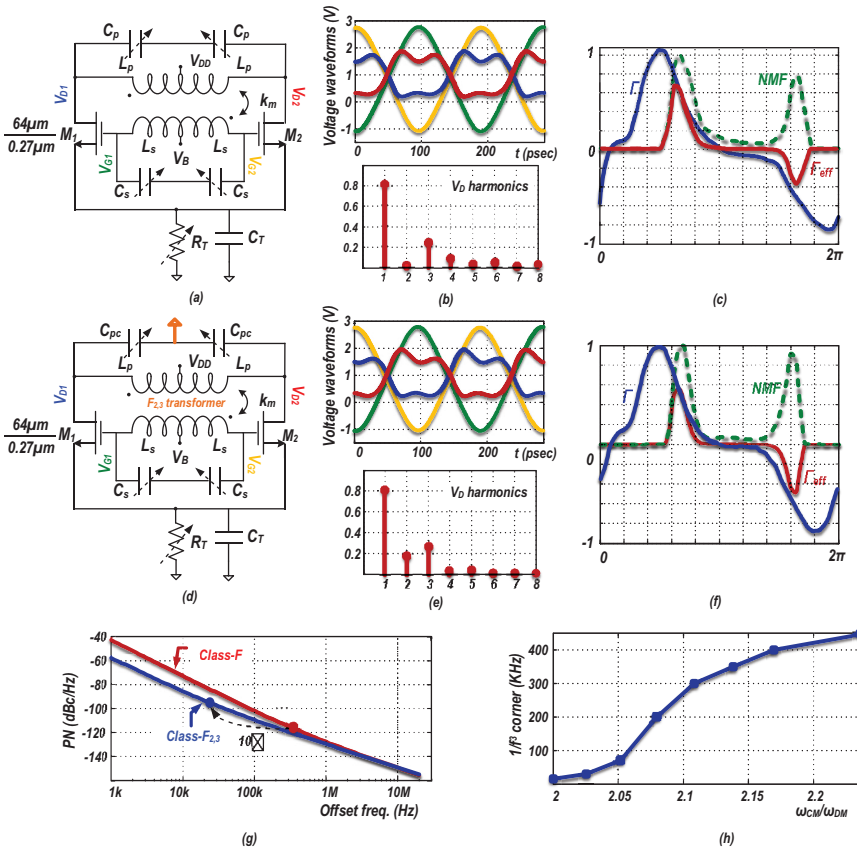

Figure 5.20 Class-F_3 oscillator: (a) schematic; (b) its waveforms; and (c) gm-transistor ISF, NMF, and effective ISF. Class-$F_{2,3}$ oscillator: (d) schematic; (e) its waveforms; and (f) gm-transistor ISF, NMF, and effective ISF; (g) their PN performance; and (h) $1/f^3$ corner sensitivity to ω_{CM}/ω_{DM}.

by creating a pseudo-square-wave oscillation waveform (see Figure 5.20(b)). We can merge our transformer-based F_2 tank with the class-F_3 operation in [5] to design a class-$F_{2,3}$ oscillator, as shown in Figure 5.20(d–e). To ensure $\omega_{CM} = 2\omega_{0,DM}$ and $\omega_{1,DM} = 3\omega_{0,DM}$, we force $L_sC_s = 3.8L_{pd}C_p$ and $k_m = 0.67$. The relatively low k_m increases the impedance at $\omega_{1,DM} \equiv 3\omega_{0,DM}$ [31]. However, the class-F_3 oscillator meets the oscillation criteria only at $\omega_{0,DM}$. Figure 5.20(e) demonstrates that the pseudo-square waveform of class-F_3 oscillation is preserved in the class-$F_{2,3}$ oscillator. The waveform does not appear to differ much; however, the oscillation voltage spectrum

indeed confirms the class-$F_{2,3}$ operation. I_{H2} is not very large in this class of oscillators, consequently, the fall/rise-time asymmetry is not as distinct as in the class-D oscillator. However, the 1/f^3 corner improvement from 400 kHz in class-F_3 to <30 kHz in class-$F_{2,3}$, as demonstrated in Figure 5.20(g), proves the effectiveness of the method. The ISF, NMF, and effective ISFs for these oscillators are shown in Figure 5.20(c,f).

Class-$F_{2,3}$ oscillator performance is sensitive to the deviation of ω_{CM} from $2\omega_0 \equiv 2\omega_{DM}$. C_p changes both CM and DM resonant frequencies while C_s only changes the DM one. To examine the robustness of the F_2 operation, differential capacitors are added in the tank's primary. Here again $C_{p,c} + C_{p,d}$ is constant to maintain the oscillation frequency. Figure 5.20(h) shows the 1/f^3 corner versus. ω_{CM}/ω_{DM} ratio and underscores the need to control the capacitance ratio, as per (5.22). Otherwise, a small deviation increases the 1/f^3 corner rapidly, and with larger deviations, the method becomes ineffective. The class-$F_{2,3}$ topology is somewhat less robust to process variations. This topology is generally more sensitive to deviations of ω_{CM} from $2\omega_0$ due to higher CM resonance quality factor. Moreover, in this topology, $\omega_{CM}/\omega_{DM} = \sqrt{((L_sC_s + L_pC_p)/(L_pC_p))}$ and is dependent on secondary and primary windings' inductance and capacitance ratio. The modification of core transistors parasitic capacitance modifies both primary and secondary capacitances and, hence, both DM and CM resonant frequencies are affected in the same direction (they are both going to increase with less parasitic capacitance and vice versa). Therefore, the ω_{CM}/ω_{DM} ratio is not affected drastically with the parasitic capacitance variations; however, due to larger Q_{CM}, the small effects are also important. Figure 5.21(a) shows the simulation results for 1/f^3 corner of the class-$F_{2,3}$ oscillator in different

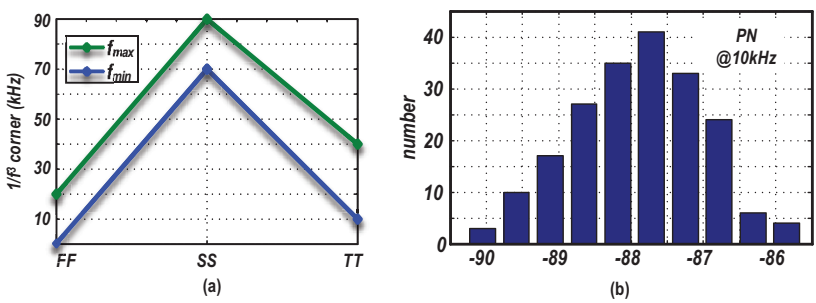

Figure 5.21 Class-$F_{2,3}$ oscillator: 1/f^3 corner over process variation and (b) histogram of PN at 10-kHz offset frequency.

process corners. The 1/f^3 corner is more affected compared to the class-D/F_2 oscillator; however, it is still very competitive. The PN at 10-kHz offset frequency for class-$F_{2,3}$ oscillator for 200 points Monte Carlo simulations on inter/intra die process variations is shown in Figure 5.21(b).

It should be worthwhile to mention that recently a mm-wave class-F_{23} oscillator considering the second-harmonic current return path was discussed in [35].

5.4 Experimental Results

The class-D/F_2 and class-$F_{2,3}$ oscillators, whose schematics were shown in Figure 5.16(d) and Figure 5.20(d), respectively, are designed in 40-nm CMOS to demonstrate the suppression of the 1/f noise upconversion. For fair comparison, we attempted to design the oscillators with the same specifications, such as center frequency, tuning range, and supply voltage, as their original reference designs in [4] and [5].

5.4.1 Class-*D*/*F*$_2$ Oscillator

The class-D/F_2 oscillator is realized in a 40-nm 1P8M CMOS process *without* ultra-thick metal layers. The two-turn inductor is constructed by stacking the $1.45\,\mu m$ Alucap layer on top of the $0.85\,\mu$m top (M8 layer) copper metal. The DM inductance is 1.5 nH with simulated Q of 12 at 3 GHz. Combination of MOS/MOM capacitors between the supply and ground is placed on-chip to minimize the effective L_T inductance, and the remaining uncompensated inductance is modeled very carefully. The capacitor bank is realized with 6-bit switchable MOM capacitors with LSB of 30 fF. The oscillator is tunable between 3.3 and 4.5 GHz (31% TR) via this capacitor bank. $M_{1,2}$ transistors are (200/0.04)-μm low-V_t devices to ensure start-up and class-D operation over PVT. The chip micrograph is shown in Figure 5.22(a) with core area of 0.1 mm^2.

Figure 5.23(a) shows the measured PN at f_{max} and f_{min} with $V_{DD} = 0.5$ V. Current consumption is 6 and 4 mA, respectively. The 1/f^3 corner is 100 kHz at f_{max} and reduces to 60 kHz for f_{min}. The 1/f^3 corner over TR is shown in Figure 5.23(c). The supply frequency pushing is 60 and 40 MHz/V at f_{max} and f_{min}, respectively (see Figure 5.23(b)). Table 5.1 compares its performance with the original class-D oscillators (as well as two other relevant oscillators [21, 26] aimed at reducing the 1/f noise upconversion).

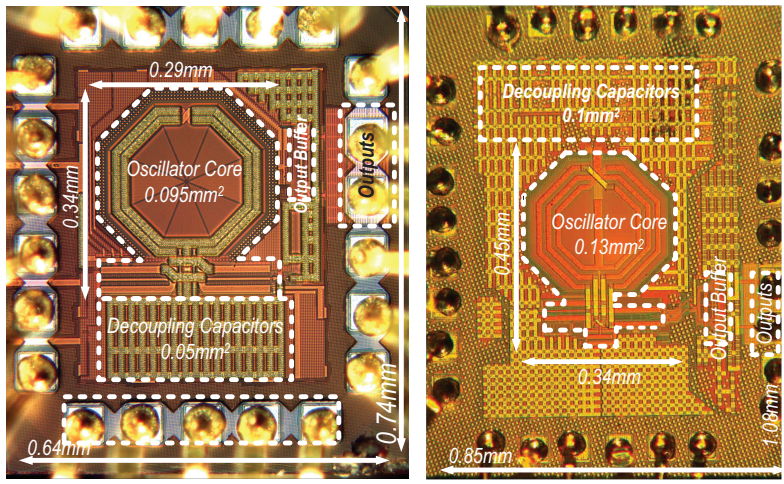

Figure 5.22 Chip micrographs: (a) class-D/F_2 oscillator; (b) class-$F_{2,3}$ oscillator.

Compared to the original design, the FoM at 10-MHz offset is degraded in the class-D/F_2 oscillator by 3 dB, mainly due to the lack of ultra-thick metal layers, which lowers the inductor's Q. However, even with this degradation, FoM at 100-kHz offset is improved at least 3 dB. $1/f^3$ corner is improved at least 10 times versus both class-D and noise-filtering class-D oscillators.

5.4.2 Class-$F_{2,3}$ Oscillator

The class-$F_{2,3}$ oscillator is realized in 40-nm 1P7 CMOS process with ultra-thick metal layer. The 1:2 transformer is constructed with the 3.4 μm top ultra-thick (M7 layer) copper metal. The primary and secondary winding inductances are 0.58 and 1.5 nH, respectively, and $k_m = 0.67$. The simulated Q-factors of the primary and secondary windings are 15 and 20 at 6 GHz. Like the class-D/F_2, the L_T inductance has to be compensated with enough decoupling capacitance. The unfiltered part has to be modeled precisely due to the relatively large R_{p2}. The single-ended primary and differential secondary capacitor banks are realized with two 6-bit switchable MOM capacitors with LSB of 30 fF and 50 fF, respectively. Due to the sensitivity of this oscillator to the frequency mismatch, an 8-bit unit-weighted capacitor bank with LSB of 4 fF is also placed at the primary to tune the DM and CM resonance frequencies. The oscillator is tunable between 5.4

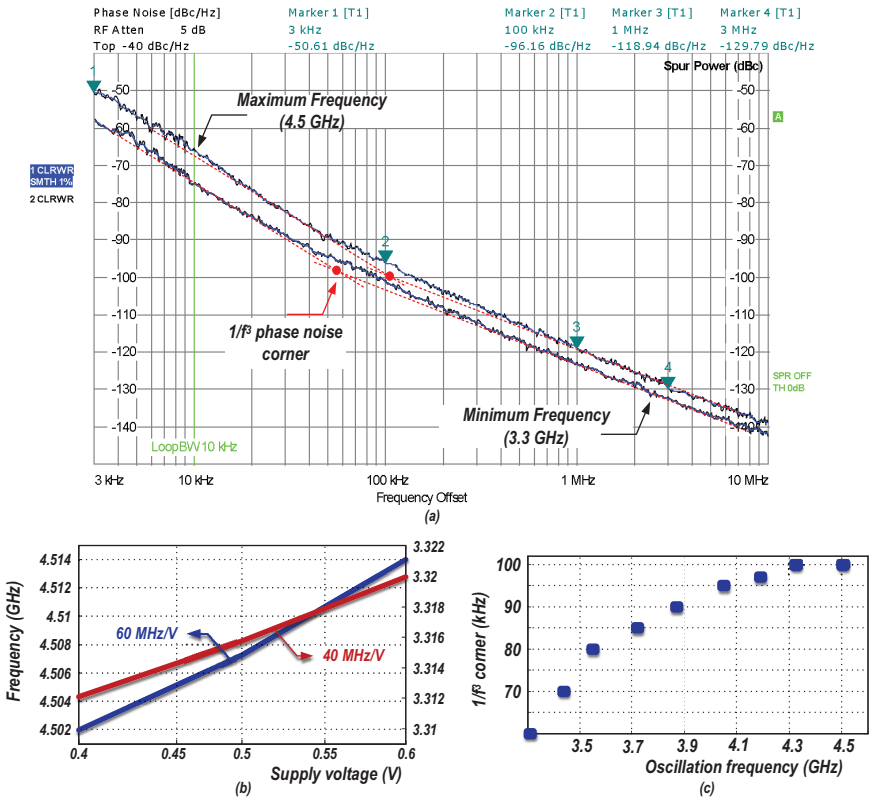

Figure 5.23 Class-D/F_2 oscillator: measured (a) PN at f_{max} and f_{min}; (b) frequency pushing due to supply voltage variation; and (c) 1/f^3 corner over tuning range.

Table 5.1 Performance summary and comparison with relevant oscillators

		Class-D/F_2		Class-D [4]		Noise filtering Class-D [4]		**Class-$F_{2,3}$**		Class-F_3[5]	[21]	[26]	[33]
Technology		**40 nm**		65 nm		65 nm		**40 nm**		65 nm	0.35 µm BiCMOS	65 nm	28 nm
Thick metal		**No**		Yes		Yes		**Yes**		Yes	NA	NA	NA
V_{DD} (V)		**0.5**		0.4		0.4		**1**		1.25	2.7	1.2	0.9
Tuning range (%)		**31**		45		45		**25**		25	14	18	27.2
Core area (mm^2)		**0.1**		0.12		0.15		**0.13**		0.12	NA	0.08	0.19
Freq. (GHz)		**f_{min}**	**f_{max}**	f_{min}	f_{max}	f_{min}	f_{max}	**f_{min}**	**f_{max}**	f_{max}	f_{mid}	f_{max}	f_{mid}
		3.3	**4.5**	3	4.8	3	4.8	**5.4**	**7**	7.4	1.5	3.6	3.3
P_{DC} (mW)		**4.1**	**2.5**	6.8	4	6.8	3.6	**12**	**10**	15	16.2	0.72	6.8
PN (dBc /Hz)	100kHz	**-101.2**	**-96.2**	-101	-91	-102	-92.5	**105.3**	**102.1**	-98.5	-110	-94.4	-106
	1MHz	**-123.4**	**-119**	-127	-119	-128	-121	**126.7**	**124.5**	-125	132	-114.4	-130
	10MHz	**-143.4**	**-139**	-149.5	-143.5	-150	-144.5	**146.7**	**144.5**	-147	NA	-134.5	-150
FoM† (dB)	100kHz	**185.4**	**185.3**	182.2	178.6	183.2	180.6	**189.1**	**188.9**	184.1	181.5	186.8	188.1
	1MHz	**187.6**	**188**	188.2	186.6	189.2	189.1	**190.5**	**191.4**	190.6	183.5	186.9	192.2
	10MHz	**187.6**	**188**	190.7	191.1	191.2	192.6	**190.5**	**191.4**	192.6	NA	187	192.2
1/f^3 corner (kHz)		**60**	**100**	800	2100	650	1500	**60**	**130**	700	11	10	200
Freq. pushing (MHz/V)		**40 @0.5 V**	**60 @0.5 V**	140 @0.5 V	480 @0.5 V	90 @0.5 V	390 @0.5 V	**12 @1V**	**23 @1V**	50 @1.25 V	NA	15 @1.2 V	NA

†*FOM*= $|PN|+20\ log_{10}(\omega_0/\Delta\omega)-10\ log_{10}(P_{DC}/1mW)$.

and 7 GHz and the primary and secondary capacitors are changed simultaneously to preserve the class-$F_{2,3}$ operation. The $M_{1,2}$ transistors are (64/0.27) μm thick-oxide devices to tolerate large voltage swings. The tail resistor R_T bank is realized with a fixed 40-Ω resistor in parallel with 7-bit binary-weighted switchable resistors with LSB size of 5 Ω. This bank can tune the oscillation current from 5–20 mA. The chip micrograph is shown in Figure 5.22(b); the core die area is 0.12 mm^2.

Figure 5.24(a) shows the measured PN of the class-$F_{2,3}$ oscillator at f_{max} and f_{min} with $V_{DD} = 1$ V. Current consumption is 10 and 12 mA, respectively. The 1/f^3 corner is 130 kHz at f_{max} and reduces to ~60 kHz at f_{min}. The 1/f^3 corner over TR is plotted in Figure 5.24(c). The supply frequency pushing is 23 and 12 MHz/V at f_{max} and f_{min}, respectively (see Figure 5.24(b)). Table 5.1 compares its performance with the original class-F_3

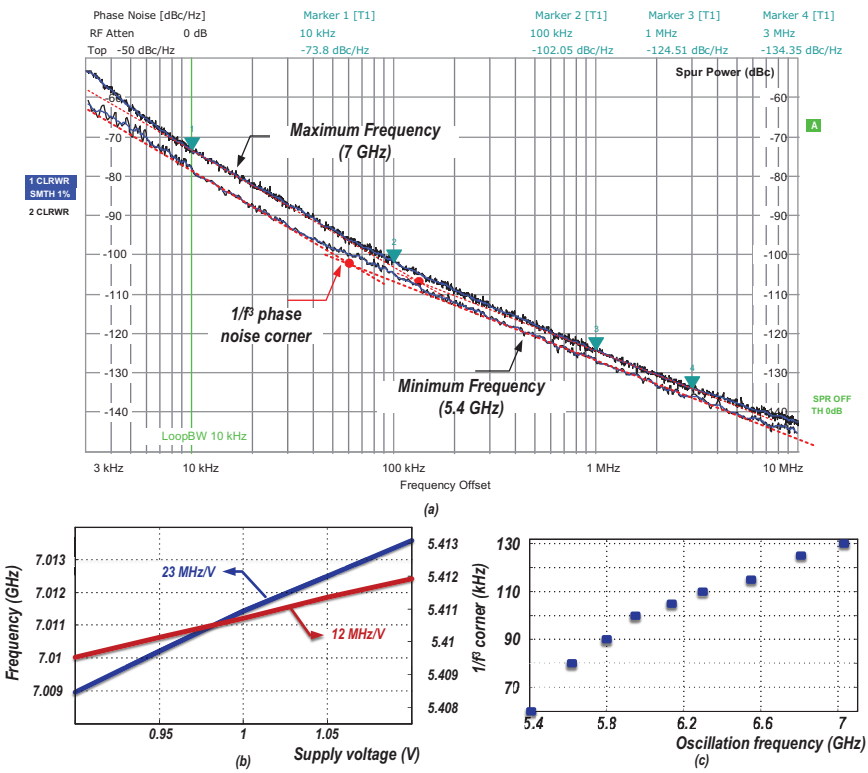

Figure 5.24 Class-$F_{2,3}$ oscillator: measured (a) PN at f_{max} and f_{min}; (b) frequency pushing due to supply voltage variation; and (c) 1/f^3 corner over tuning range.

oscillator. Compared to the original design, FoM is degraded about 1–2 dB at the 10-MHz offset, which is due to the tail resistor loading the tank more than the tail transistor originally, thus degrading PN slightly. Despite this degradation, FoM at 100 kHz is enhanced by at least 4 dB, and the $1/f^3$ corner is improved 5 times.

It might be interesting to point out that class-$F_{2,3}$ oscillator was adapted for an operation at cryogenic temperatures of 4K [36] where it exhibited a record-low 1/f corner.

5.5 Conclusion

In this chapter, we discussed and analyzed a technique to reduce a 1/f noise upconversion in a harmonically rich tank current. We showed that when even-order harmonics of the tank current flow into the capacitive part of the tank, they distort the oscillation waveform by making its rise and fall times asymmetric and hence causing the 1/f noise upconversion. Odd-order harmonics also distort the oscillation waveform; however, the waveform in that case is still symmetric and will not result in the 1/f noise upconversion. We showed how to design a ω_0-tank that shows an auxiliary common-mode (CM) resonant peak at $2\omega_0$, which is the main contributor to the 1/f noise upconversion, and showed how oscillation waveform becomes symmetric by the auxiliary resonance. We described how to realize the F_2-tank without the die area penalty, by taking advantage of different properties of inductors and transformers in differential-mode (DM) and CM excitations. Class-D/F_2 and class-$F_{2,3}$ oscillators employing, respectively, inductor- and transformer-based F_2 tanks are designed in 40-nm CMOS to show the effectiveness of our proposed method. The $1/f^3$ corner improves $10\times$ in class-D/F_2 and $5\times$ in class-$F_{2,3}$ versus their original counterparts.

References

[1] H. Darabi, H. Jensen, and A. Zolfaghari, "Analysis and design of small-signal polar transmitters for cellular applications," *IEEE J. Solid-State Circuits*, vol. 46, no. 6, pp. 1237–1249, June 2011.

[2] D. Tasca et al., "A 2.9-4.0 GHz fractional-N digital PLL with bang-bang phase detector and 560-fs rms integrated jitter at 4.5-mW power," *IEEE J. Solid-State Circuits*, vol. 44, no. 12, pp. 2745–2758, Dec. 2011.

[3] L. Fanori and P. Andreani, "Highly efficient class-C CMOS VCOs, including a comparison with class-B VCOs," *IEEE J. Solid-State Circuits*, vol. 48, no.7, pp. 1730–1740, Jul. 2013.

[4] L. Fanori and P. Andreani, "Class-D CMOS oscillators," *IEEE J. Solid-State Circuits*, vol. 48, no. 12, pp. 3105–3119, Dec. 2013.

[5] M. Babaie and R. B. Staszewski, "A class-F CMOS oscillator," *IEEE J. Solid-State Circuits*, vol. 48, no. 12, pp. 3120–3133, Dec. 2013.

[6] E. Hegazi and A. A. Abidi, "Varactor characteristics, oscillator tuning curves, and AM-FM conversion," *IEEE J. Solid-State Circuits*, vol. 38, no. 6, pp. 1033–1039, Jun. 2003.

[7] B. Soltanian and P. Kinget, "AM-FM conversion by the active devices in MOS LC-VCOs and its effect on the optimal amplitude," *IEEE Radio Frequency Integrated Circuits Symp.*, Jun. 2006.

[8] S. Levantino et al., "Frequency dependence on bias current in 5-GHz CMOS VCO's: Impact of tuning range and flicker noise up-conversion," *IEEE J. Solid-State Circuits*, vol. 37, no. 8, pp. 1003–1011, Aug. 2002.

[9] Y. Hu, T. Siriburanon, and R. B. Staszewski, "Intuitive understanding of flicker noise reduction via narrowing of conduction angle in voltage-biased oscillators", *IEEE Trans. on Circuits and Systems II (TCAS-II)*, pp. 1–5, 2019.

[10] J. Groszkowski, "The impedance of frequency variation and harmonic content, and the problem of constant-frequency oscillator," *Proc. IRE*, vol. 21, pp. 958–981, 1933.

[11] A. Bevilacqua and P. Andreani, "On the bias noise to phase noise conversion in harmonic oscillators using Groszkowski theory," *IEEE Int. Symp. Circuits Syst.*, 2011, pp. 217–220.

[12] J. Rael and A. Abidi, "Physical processes of phase noise in differential LC oscillators," *in Proc. IEEE Custom Integr. Circuits Conf.*, Sept. 2000, pp. 569–572.

[13] A. Hajimiri and T. H. Lee, "A general theory of phase noise in electrical oscillators," *IEEE J. Solid-State Circuits*, vol. 33, no. 2, pp. 179–194, Feb. 1998.

[14] J. E. Post, I. R. Linscott, and M. H. Oslick, "Waveform symmetry properties and phase noise in oscillators," *Electron. Lett.*, vol. 34, no. 16, pp. 1547–1548, Aug. 1998.

[15] D. Murphy, J. J. Rael, and A. A. Abidi, "Phase noise in LC oscillators: A phasor-based analysis of a general result and of loaded Q," *IEEE Trans. Circuits Syst. I, Reg. Papers*, vol. 57, no. 6, pp. 1187–1203, June 2010.

[16] A. Bevilacqua and P. Andreani, "An analysis of 1/f noise to phase noise conversion in CMOS harmonic oscillators," *IEEE Trans. Circuits Syst. I, Reg. Papers*, vol. 59, no. 5, pp. 938–945, May 2012.

[17] E. A. Vittoz, M. G. R. Degrauwe, and S. Bitz, "High-performance crystal oscillator circuits: theory and application," *IEEE J. Solid-State Circuits*, vol. 23, no. 3, pp. 774–783, Jun. 1988.

[18] M. A. Margarit, J. L. Tham, R. G. Meyer, and M. J. Deen, "A low-noise, low-power VCO with automatic amplitude control for wireless applications," *IEEE J. Solid-State Circuits*, vol. 34, no. 6, pp. 761–771, Jun. 1999.

[19] A. R. Jeng and C. G. Sodini, "The impact of device type and sizing on phase noise mechanisms" *IEEE J. Solid-State Circuits*, vol. 40, no. 2, pp. 360–369, Feb. 2005.

[20] S.-J. Yun, C. Y. Cha, H. C. Choi, and S. G. Lee, "RF CMOS LC-oscillator with source damping resistors," *IEEE Microw. Wireless Compon. Lett.*, vol. 16, no. 9, pp. 511–513, Sep. 2006.

[21] F. Pepe, A. Bonfanti, S. Levantino, C. Samori, and A. L. Lacaita, "Suppression of flicker noise up-conversion in a 65-nm CMOS VCO in the 3-to-3.6 GHz band," *IEEE J. Solid-State Circuits*, vol. 48, no. 10, pp. 2375–2389, Oct. 2013.

[22] M. Shahmohammadi, M. Babaie, and R. B. Staszewski, "A 1/f noise up-conversion reduction technique applied to class-D and class-F oscillators," *in IEEE Int. Solid-State Circuits Conf. Dig Tech. Papers (ISSCC)*, Feb. 2015, pp. 444–445.

[23] M. Shahmohammadi, M. Babaie, and R. B. Statszewsi, "A 1/f noise upconversion reduction technique for voltage-biased RF CMOS oscillators," *IEEE J. Solid-State Circuits*, vol. 51, no. 11, pp. 2610–2624, Nov. 2016.

[24] P. Andreani, X. Wang, L. Vandi, and A. Fard, "A study of phase noise in Colpitts and LC-tank CMOS oscillators," *IEEE J. Solid-State Circuits*, vol. 40, no. 5, pp. 1107–1118, May 2005.

[25] Z. Zong, P. Chen, and R. B. Staszewski, "A Low-noise fractional-N digital frequency synthesizer with implicit frequency tripling for mm-Wave applications," *IEEE J. Solid-State Circuits*, vol. 54, no. 3, pp. 755–767, Mar. 2019.

[26] D. Murphy, H. Darabi, and H. Wu, "A VCO with implicit common mode resonance," *in IEEE Int. Solid-State Circuits Conf. Dig Tech. Papers (ISSCC)*, Feb. 2015, pp. 442–443.

[27] D. Murphy, H. Darabi, and H. Wu, "Implicit common-mode resonance in LC oscillators," *IEEE J. Solid-State Circuits*, vol. 52, no. 3, pp. 812–821, Mar. 2017.

[28] J. Chen et al., "A Digitally Modulated mm-Wave Cartesian Beamforming Transmitter with Quadrature Spatial Combining," *in IEEE Int. Solid-State Circuits Conf. Dig Tech. Papers (ISSCC)*, Feb. 2013, pp. 232–233.

[29] D. Chowdhury, L. Ye, E. Alon, and A. M. Niknejad, "An efficient mixed-signal 2.4-GHz polar power amplifier in 65-nm CMOS technology," *IEEE J. Solid-State Circuits*, vol. 46, no. 8, pp. 1796–1809, Aug. 2011.

[30] M. Babaie and R. B. Staszewski, "An ultra-low phase noise class-F2 CMOS oscillator with 191 dBc/Hz FOM and long term reliability," *IEEE J. Solid-State Circuits*, vol. 50, no. 3, pp. 679–692, Mar. 2015.

[31] A. Mazzanti and A. Bevilacqua, "On the phase noise performance of transformer-based CMOS differential-pair harmonic oscillators," *IEEE Trans. Circuits Syst. I, Reg. Papers*, vol. 62, no. 9, pp. 2334–2341, Sep. 2015.

[32] E. Hegazi, H. Sjoland, and A. A. Abidi, "A filtering technique to lower LC oscillator phase noise," *IEEE J. Solid-State Circuits*, vol. 36, no. 12, pp. 1921–1930, Dec. 2001.

[33] A. Mostajeran, M. Sharif Bakhtiar, and E. Afshari, "A 2.4 GHz VCO with FOM of 190 dBc/Hz at 10kHz-to-2MHz offset frequencies in 0.13 μm CMOS using an ISF manipulation technique," *in IEEE Int. Solid-State Circuits Conf. Dig Tech. Papers (ISSCC)*, Feb. 2015, pp. 452–453.

[34] M. Shahmohammadi, M. Babaie, and R. B. Staszewski, "Resonator circuit," *US Patent Application 2017/0366137*, published 21 Dec. 2017.

[35] Y. Hu, T. Siriburanon, and R. B. Staszewski, "A low-flicker-noise 30-GHz class-F_{23} oscillator in 28-nm CMOS using implicit resonance and explicit common-mode return path," *IEEE Journal of Solid-State Circuits (JSSC)*, vol. 53, no. 7, pp. 1977–1987, July 2018.

[36] B. Patra, R. M. Incandela, J. P. G. van Dijk, H. A. R. Homulle, L. Song, M. Shahmohammadi, R. B. Staszewski, A. Vladimirescu, M. Babaie, F. Sebastiano, and E. Charbon, "Cryo-CMOS circuits and systems for quantum computing applications," *IEEE Journal of Solid-State Circuits (JSSC)*, vol. 53, no. 1, pp. 309–321, Jan. 2018.